

Simulation of Interaction-Induced Chiral Topological Dynamics on a Digital Quantum Computer

Jin Ming Koh¹, Tommy Tai,^{2,3} and Ching Hua Lee^{1,3,*}

¹*Division of Physics, Mathematics and Astronomy, Caltech, Pasadena, California 91125, USA*

²*Cavendish Laboratory, University of Cambridge, JJ Thomson Avenue, Cambridge CB3 0HE, United Kingdom*

³*Department of Physics, National University of Singapore, Singapore 117542*



(Received 27 February 2022; revised 30 June 2022; accepted 2 September 2022; published 28 September 2022)

Chiral edge states are highly sought after as paradigmatic topological states relevant to both quantum information processing and dissipationless electron transport. Using superconducting transmon-based quantum computers, we demonstrate chiral topological propagation that is induced by suitably designed interactions, instead of flux or spin-orbit coupling. Also different from conventional 2D realizations, our effective Chern lattice is implemented on a much smaller equivalent 1D spin chain, with sequences of entangling gates encapsulating the required time-reversal breaking. By taking advantage of the quantum nature of the platform, we circumvented difficulties from the limited qubit number and gate fidelity in present-day noisy intermediate-scale quantum era quantum computers, paving the way for the quantum simulation of more sophisticated topological states on very rapidly developing quantum hardware.

DOI: 10.1103/PhysRevLett.129.140502

Introduction.—The discovery of the integer quantum Hall effect in 2D electron gases revolutionized condensed-matter physics [1,2]. To circumvent the requirement of a strong external magnetic field, tight-binding lattices with intrinsic time-reversal symmetry (TRS) breaking have been devised, inspired by Haldane’s seminal Chern insulator [3]. Such lattice-based chiral topological phenomenon is known as the “quantum anomalous Hall effect” and has been demonstrated in ferromagnetic topological insulators [4–7], magic-angle twisted bilayer graphene [8–11], and moiré heterostructures [12–14]. Such is their academic and potential technological impact that topological boundary states have also been realized in photonic platforms [15–23] and polariton [24–27], mechanical gyrotopic [28–30], and acoustic [19,31–35] systems, as well as topoelectrical circuits [36–53].

In the above, the broken TRS required for chiral topological propagation has been introduced through magnetic dopants, orbital magnetism, or nonreciprocal media. Tantalizing alternative routes, however, exist when the chiral lattice is physically implemented on universal quantum simulators, as in quantum circuits and quantum computers [54–60]. In particular, such fully quantum platforms have the innate propensity to realize the non-trivial TRS-breaking topology via novel many-body effects and interactions. In this Letter, we hence demonstrate how chiral topological dynamics can be induced through engineered interactions, rather than conventional single-body mechanisms such as spin-orbit coupling.

As intrinsically quantum platforms, quantum computers are, in principle, able to realize any quantum phenomenon, including strong interaction effects beyond the reach of

classical topological metamaterials. Even in the current noisy intermediate-scale quantum (NISQ) era, digital quantum computers have shown incredible promise [61–65] due to their versatility, complementing alternative experimental platforms such as ultracold polar molecules [66,67] and Rydberg atoms [68–70]. Programmable with universal quantum gate sets that can simulate generic unitaries, quantum computers are ideally poised as platforms for observing various condensed-matter and topological phenomena, particularly those that require esoteric or many-body coupling configurations. Existing bottlenecks, such as low gate fidelity, decoherence, limited qubit connectivity, and limited number of qubits [71], may be significantly alleviated by error mitigation and circuit optimization techniques [72–76].

To date, simulating two-dimensional systems such as Chern lattices has been inherently challenging given the aforementioned hardware constraints. Physical simulations on digital quantum computers have largely been restricted to 1D spin or fermionic chains and small 2D systems [77–83]. Indeed, due to the numerous lattice sites ($\gtrsim 10^2$) necessary for cleanly observing chiral mode propagation, these paradigmatic topological states have been missing from quantum computer demonstrations.

In this Letter, we propagate a chiral topological mode on a quantum computer, demonstrating a versatile quantum simulation setup that complements existing experimental realizations of Chern topology. By designing logical two-body interactions, the Chern lattice is mapped exactly onto a 1D chain with two interacting excitations [84], which is well within the capabilities of NISQ quantum computers. Our remapping relied on the fact that Chern topological

states are fundamentally single-body phenomena and can thus be “compressed” into a smaller physical system already hosting an exponentially large quantum many-body Hilbert space. We employed IBM transmon-based superconducting quantum computers, which have been utilized in various applications [88,89], including quantum chemistry [90,91] and spin lattice problems [79,92]. Compared to existing quantum computer simulations of other topological systems [55–57], ours is performed in physical, not synthetic, space with a significantly more complex Hamiltonian, allowing for the observation of topological boundary chiral dynamics in an intrinsically 2D setting.

Chern lattice as an interacting model.—A Chern lattice is a system with an integer C number of robust chiral boundary modes, where C is the Chern topological invariant [93]. This invariant is defined as the index of the mapping $T^2 \rightarrow \Gamma$, where Γ is the state space where eigenstates live. For two-band models, Γ takes the familiar form of the Bloch sphere, and C measures how many times the torus T^2 wraps around the sphere.

Although the torus is commonly taken to represent 2D lattice momentum space, it can also refer to the joint configuration momentum space of two particles, whose interactions correspond to effective hoppings that shape the mapping $T^2 \rightarrow \Gamma$. This alternative representation takes advantage of the much larger many-body Hilbert space intrinsically accessible on a quantum computer: unlike in classical systems, just N qubits can index up to 2^N possible configurations, thereby easily accommodating the $\mathcal{O}(N^2)$ -dimensional basis of T^2 . As such, by rewriting certain hoppings in terms of interaction terms, we can achieve drastically more compact simulations of higher-dimensional lattices. Such a mapping makes Chern boundary modes, which usually require $\mathcal{O}(10^2)$ lattice sites [94] to properly resolve, readily observable on current-generation quantum computers with $\mathcal{O}(10^1)$ high-quality interconnected qubits.

In addition to allowing for the compact simulation of physical lattices, a digital quantum computer realization is greatly versatile in accommodating couplings of differing ranges and types. For concreteness, we discuss in the context of the topological Hamiltonian that we implemented; but this versatility applies to lattice Hamiltonians in general. We used a modified version of the checkerboard lattice model well known for flat band properties and strongly correlated states [95–97], $\mathcal{H} = \sum_{\mathbf{k}} \mathcal{H}(\mathbf{k}) c_{\mathbf{k}}^\dagger c_{\mathbf{k}}$, where $\mathcal{H}(\mathbf{k}) = \mathbf{d}(\mathbf{k}) \cdot \boldsymbol{\sigma}$ =

$$\begin{bmatrix} -4v_2 \sin k_- \sin k_+ & 2v_1(\cos k_- + \cos k_+ e^{2i\phi}) \\ 2v_1(\cos k_- + \cos k_+ e^{-2i\phi}) & 4v_2 \sin k_- \sin k_+ \end{bmatrix}, \quad (1)$$

for $k_{\pm} = k_1 \pm k_2$ written in its original 2D momentum space. Above, $\mathbf{d}(\mathbf{k})$ denotes the Bloch vector (see Sec. S1 of Supplemental Material [98]) and $\boldsymbol{\sigma}$ are Pauli matrices.

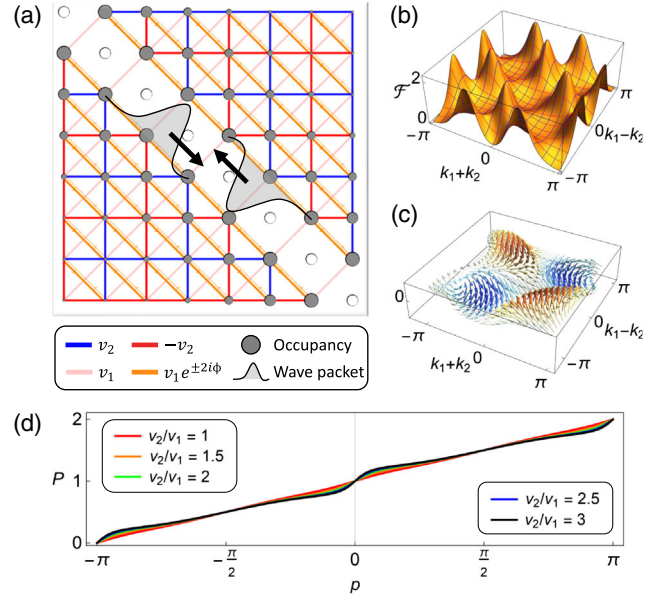


FIG. 1. Chiral topological propagation from interactions. (a) Chern topology arises from a checkerboard lattice with nonreciprocal couplings carrying effective flux (thick and thin orange arrows). Implemented as a 1D interacting chain, vertical, horizontal, and diagonal couplings become single-boson (red, blue) and two-boson hoppings (pink, orange), respectively. An on-site repulsive interaction is imposed to yield a virtual boundary along the lattice diagonal, along which chiral propagation occurs in the form of oppositely moving two-particle wave packets (black arrows). (b) The Berry curvature \mathcal{F} and (c) its corresponding $\mathbf{d}(\mathbf{k})$ -vector skyrmionic texture of our model for $v_1 = v_2 = 1$ and $\phi = \pi/6$. The total number of chiral edge modes is the Chern number $\int \mathcal{F} d^2 \mathbf{k} / 2\pi = 2$. (d) The Wannier polarization representing the center-of-mass translation of a maximally localized wave packet as we thread a flux $k_+ \rightarrow k_+ + A_y$. It is pumped $C = 2$ upon a complete cycle and moves with almost perfect uniformity for most values of the ratios v_2/v_1 .

The lattice-space representation of our Hamiltonian, obtained by a Fourier transform of Eq. (1), is exactly depicted in Fig. 1(a), consisting of two square lattices interlocked in a checkerboard fashion. This lattice contains intersublattice couplings v_1 in the directions $\Delta\mathbf{r} = (1, \pm 1)$ and $(-1, \pm 1)$. Vertical and horizontal v_2 hoppings take alternate signs in adjacent checkers [Fig. 1(a)]. Importantly, the requisite TRS breaking for Chern topology enters through the alternating phase factors $e^{\pm 2i\phi}$ along the diagonal $\Delta\mathbf{r} \propto (1, 1)$, in the couplings between the upper-lower and lower-upper sublattices. While realizing these phase factors can be challenging in conventional topological media [35,121–125], they are readily achievable on a digital quantum computer.

As the next step, we rewrite these hoppings via $c_{x_1, x_2}^\dagger \rightarrow \mu_{x_1}^\dagger \nu_{x_2}^\dagger$, where μ^\dagger and ν^\dagger create hard-core bosons of two different species in 1D, such that the $(1+1)$ -body sector of this new system \mathcal{H}_{1D} corresponds to the original 2D Hamiltonian \mathcal{H} with

$$\begin{aligned} \mathcal{H}_{1D} = & v_1 \sum_{x_1, x_2 \text{ even}} (\mu_{x_1+1}^\dagger e^{2i\phi} + \mu_{x_1-1}^\dagger) \nu_{x_2+1}^\dagger \mu_{x_1} \nu_{x_2} \\ & + v_1 \sum_{x_1, x_2 \text{ odd}} (\mu_{x_1+1}^\dagger e^{-2i\phi} + \mu_{x_1-1}^\dagger) \nu_{x_2+1}^\dagger \mu_{x_1} \nu_{x_2} \\ & + v_2 \sum_x (-1)^x (\mu_{x+2}^\dagger \mu_x - \nu_{x+2}^\dagger \nu_x) + \text{H.c.} \end{aligned} \quad (2)$$

In this formulation, the v_2 hoppings, which were originally vertical or horizontal, remain single-body, albeit over next nearest neighbors. However, the diagonal v_1 hoppings become simultaneous two-body hopping interactions, some containing phase rotations $e^{\pm 2i\phi}$. Further, the impenetrability of the hard-core μ, ν bosons (see Sec. S1 of Supplemental Material [98]) enforces a virtual boundary that prohibits double-site occupancy along $x_1 = x_2$, i.e., the diagonal line perpendicular to k_- . The interference of the phase rotations collude to give rise to chiral topological transport along this boundary. This is apparent upon referring to the polarization

$$P(p_+) = \frac{1}{4\pi} \int_{-\pi}^{p_+} \int_{-\pi}^{\pi} \mathcal{F}(k_+, k_-) dk_- dk_+, \quad (3)$$

which changes by $C = 2$ sites upon a complete cycle of flux threading [Fig. 1(d)], implying nontrivial topological pumping. Here, $\mathcal{F} = -i\langle \partial_{x_1}\psi | \partial_{x_2}\psi \rangle + \text{H.c.}$ is the Berry curvature [126], computed from the Jacobian determinant of the $\mathbf{d}(\mathbf{k})$ mapping [Figs. 1(c) and 1(d)]. Physically, P reflects the spectral flow propagation of Wannier centers [127–130] upon flux threading and, for this model, can be optimized to be as uniform as possible to facilitate uniform chiral boundary propagation (see Sec. S1 of Supplemental Material [98]). In terms of the μ, ν bosons, this pumping is manifested as the motion of correlated particle pairs occupying adjacent sites, which is robustly protected by the flux asymmetry caused by the dissimilar effects of the phases ϕ on the left and the right of each boson. Along the virtual boundary, where the two bosons are next to each other, this asymmetry leads to a correlated pumping of their center of mass, i.e., chiral propagation.

Realization on a quantum computer.—To simulate chiral propagation, we implement \mathcal{H}_{1D} on IBM transmon-based quantum computers [131–133]. The quantum nature of this platform allows many-body systems to be directly simulated; in the present context of \mathcal{H}_{1D} , we represent each unit cell of the Chern lattice model with 2 qubits, for a total of 16 qubits representing an $L = 8$ lattice. This is a considerable reduction from the $8^2 = 64$ qubits otherwise needed, without the dimensional reduction into a 1D system. We use 27-qubit quantum devices in our simulation runs (see Sec. S2 of Supplemental Material [98]).

We map the $\{|00\rangle, |01\rangle, |10\rangle\}$ computational basis states of each pair of qubits to unoccupied, occupied by a μ boson, and occupied by a ν boson states of the model. The hard-core bosonic constraint is enforced by an appropriate

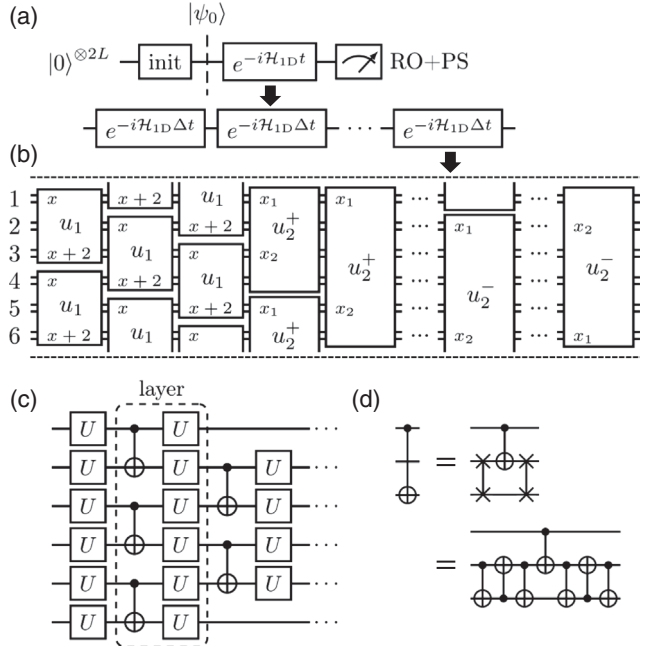


FIG. 2. Quantum circuit implementation schematics. (a) Schematic of quantum circuit for time evolving an initial state $|\psi_0\rangle$ according to our Hamiltonian \mathcal{H}_{1D} , with readout error mitigation (RO) and postselection (PS) applied on the final measurements. (b) In-principle first-order Trotterization of the $e^{-i\mathcal{H}_{1D}t}$ propagator and the breakdown of a Trotter step in terms of unitaries u_1 and u_2 , as further elaborated in Sec. S2 of Supplemental Material [98]. Pairs of qubits (drawn as double lines) represent each site of the logical Chern lattice. (c) Circuit ansatz for recompilation, comprising layers of entangling CXs and single-qubit rotations, stacked in brickwork pattern. (d) Non-nearest-neighbor CX gates can be implemented using SWAPs, which themselves decompose into nearest-neighbor CXs.

representation of μ, ν operators satisfying the canonical mixed-commutation relations. An initial state $|\psi_0\rangle$ evolves over time as $|\psi(t)\rangle = U(t)|\psi_0\rangle$, with propagator $U(t) = e^{-i\mathcal{H}_{1D}t}$. To study state dynamics on the quantum computer, it is necessary to implement $U(t)$ as a quantum circuit; a standard method is to decompose $\mathcal{H}_{1D} = \sum_\gamma A_\gamma \sigma^\gamma$ in the spin-1/2 basis, for generically noncommuting Pauli strings σ^γ and $A_\gamma \in \mathbb{R}$, and employ Trotterization [134,135]. In the first-order scheme, we split $e^{-i\mathcal{H}_{1D}t} = (e^{-i\mathcal{H}_{1D}\Delta t})^n$ into n steps, each of which is approximated as $\prod_\gamma e^{-iA_\gamma \sigma^\gamma \Delta t}$. Here, it is convenient to separate $\mathcal{H}_{1D} = h_1 + h_2$, such that h_1 contains the single-boson hoppings, and h_2 contains the two-boson interactions. Then the Trotterized circuit can be constructed from unitaries u_1 and u_2 , respectively, implementing evolution by h_1 and h_2 , as shown in Fig. 2(b). See Sec. S2 of Supplemental Material [98] for further details.

Although the physical couplings between the hardware qubits are only between nearest neighbors, long-ranged entangling gates corresponding to distant couplings in u_1 and u_2 can be effected with the application of SWAP gates.

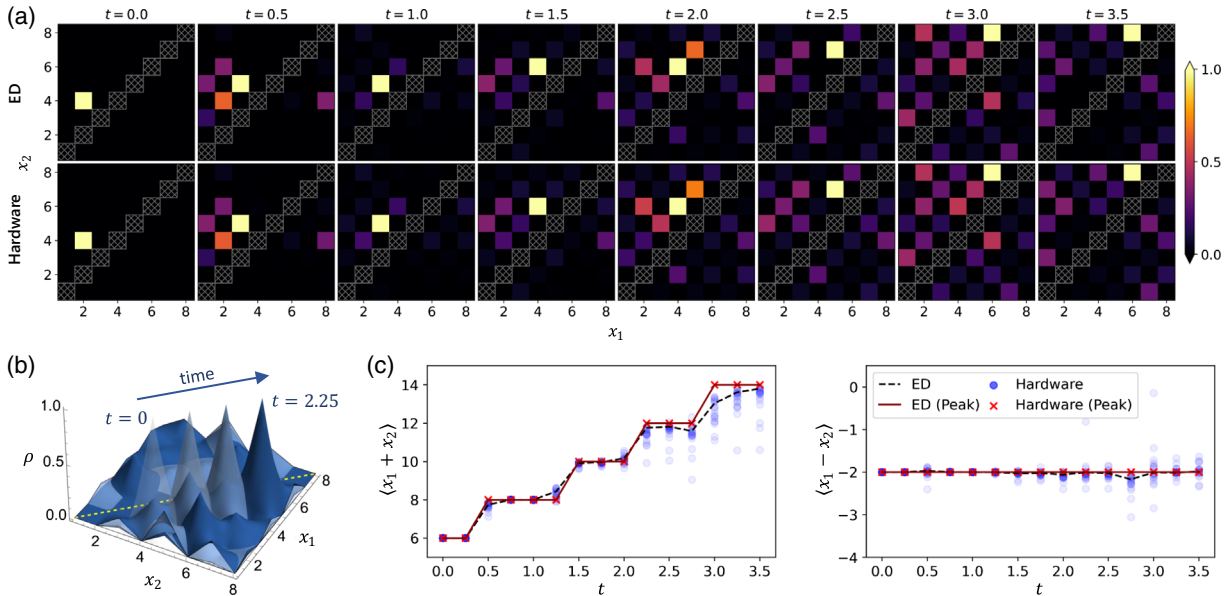


FIG. 3. Demonstration of chiral topological propagation on a quantum computer. (a) Evolution of occupancy densities $\rho(x_1, x_2) = \langle \mu_{x_1}^\dagger \mu_{x_1} \nu_{x_2}^\dagger \nu_{x_2} \rangle$ as time progresses, with good agreement between exact diagonalization (top row) and hardware data (bottom row), for an initial wave packet at $(x_1, x_2) = (2, 4)$. We have normalized the peak of $\rho(x_1, x_2)$ for visual clarity. Hatch-shaded squares indicate the $x_1 = x_2$ virtual boundary. (b) 3D visualization of the same chiral propagation, which clearly reveals the peak translating parallel to the $x_1 = x_2$ virtual boundary. The sequence of snapshots of measured $\rho(x_1, x_2)$ at $t = 0, 0.75, 1.50$, and 2.25 are superimposed (lightest to darkest). (c) Left: monotonic evolution of the center of mass $\langle x_1 + x_2 \rangle$, with localized peak positions (crosses) shifting together with the density profile (blue) and centroid $\langle x_1 + x_2 \rangle = \sum_{x_1, x_2} (x_1 + x_2) \rho(x_1, x_2)^4$ (dashed). Exact diagonalization (ED) results agree closely with data from the quantum hardware. Right: the state remains close to the diagonal virtual boundary, as indicated by constant $\langle x_1 - x_2 \rangle = 2$ over time. Parameters are $v_1 = v_2 = 1$ and $\phi = \pi/6$.

For instance, at the basic level, non-nearest-neighbor CX gates can be effected by chaining CXs on adjacent qubits [Fig. 2(d)]. The single-particle hoppings and two-particle quartic interactions are treated on equal footing in the quantum circuit implementation, and the simulation is digital in nature, compared to the aforementioned analog classical platforms [15–17,19,28–39,45,136,137].

We note, however, that in this form, the Trotterized circuits for \mathcal{H}_{1D} are infeasibly deep for current NISQ-era devices. Present benchmarks indicate $\mathcal{O}(10^2)$ CX layers are achievable with state-of-the-art techniques and hardware, likely yet smaller for quantitatively accurate simulations; the numerous Trotter steps required for acceptable truncation error easily exceeds this limit. We thus employ an implementation strategy known as circuit recompilation [59,138–140] to compress circuit depth. A circuit ansatz [Fig. 2(c)] comprising layers of single-qubit rotations and CX entangling gates, laid in a brickwork pattern, is iteratively optimized through tensor network-aided quantum simulation [141] to approach the intended unitary. Specifically, we collect the rotation angles $\boldsymbol{\vartheta} = (\boldsymbol{\theta}, \boldsymbol{\phi}, \boldsymbol{\lambda})$ and numerically treat the optimization problem $\text{argmax}_{\boldsymbol{\vartheta}} |\langle \psi_0 | V_{\boldsymbol{\vartheta}}^\dagger U | \psi_0 \rangle|^2$ for circuit unitary $V_{\boldsymbol{\vartheta}}$. Additionally, we note \mathcal{H}_{1D} is number conserving in both the μ and ν species and also conserves the parity of $x_1 + x_2$. As our focus is in states $|\psi_0\rangle$ with definite μ, ν -particle numbers and $x_1 + x_2$ parity (corresponding to

the single-particle sector on the checkerboard lattice), we need only perform calculations over the symmetry-restricted sector, significantly alleviating costs. This sector-specific recompilation technique hugely reduces circuit depth (to ≤ 12 CX layers) and is critical in our realization of the \mathcal{H}_{1D} model on present hardware. See Sec. S2 of Supplemental Material [98] for technical details.

To suppress the effects of hardware noise, we employ readout error mitigation [72–74], postselection [79,142], and averaging across qubit chains and machines. In particular, we run calibration circuits alongside each experiment and approximately correct measurement bit-flip errors via linear inversion; to feasibly accommodate 16 qubits, we use an approximate tensored scheme [59]. Finally, results that violate the μ, ν -particle number and $x_1 + x_2$ parity symmetries of \mathcal{H}_{1D} are nonphysical, enabling a postselection policy at no additional circuit depth or measurement costs.

Measured results.—We directly measured interaction-induced topological chiral propagation (Fig. 3) along a diagonal virtual boundary $x_1 = x_2$ in configuration space. We simulate the time evolution of an initial state localized at position $(x_1, x_2) = (2, 4)$ adjacent to the diagonal; an analogous set of results for $(x_1, x_2) = (7, 5)$ on the opposite side of the diagonal is given in Sec. S3 of Supplemental Material [98]. In both, the site-resolved occupancy

densities $\rho(x_1, x_2)$ measured on hardware very closely match exact diagonalization results. The chiral nature of the boundary-localized propagating modes are more saliently presented in Figs. 3(b)–3(d), where unidirectional propagation along the diagonal, in opposite directions for the two initial states, is clearly observed, as indeed expected. The unidirectionality of transport is apparent from the movement of the wave packet peak, which closely tracks $\langle x_1 + x_2 \rangle$ and monotonously increases; localization along the virtual boundary is maintained throughout transport, as verified by an almost constant $\langle x_1 - x_2 \rangle$.

While the presently studied model is interesting as it hosts chiral modes under periodic boundary conditions without physical edges, we demonstrate chiral propagation also under more traditional open boundary conditions (see Sec. S3 of Supplemental Material [98]). On such a lattice, boundary-localized wave packets unidirectionally propagate along the virtual boundary of the diagonal, bend at the corner and travel along the physical edges, and loop back onto the diagonal. In both cases, we successfully demonstrate quantum anomalous Hall-type topological transport on a fully programmable quantum platform, despite the inherent limitations of current-day NISQ-era devices.

Discussion.—In this Letter, we successfully demonstrated chiral propagating modes on a quantum computer. While observing such Chern propagation typically requires implementing 2D quantum anomalous Hall lattices, we instead employed a checkerboard model that maps into a 1D interacting chain with Pauli-like repulsive interactions. Through a combination of remapping the lattice to a spin chain and the use of appropriately designed many-body interactions [44,143], we were able to circumvent circuit breadth limitations on present-day NISQ-era quantum computers.

Indeed, quantum computers provide a versatile platform for investigating new condensed-matter phenomena, including those involving long-ranged or exotic many-body couplings. With a Hilbert space that harbors exponentially many degrees of freedom, they can accommodate various phenomena such as many-body scars, quantum phase transitions, and time crystals, even when the requisite interactions are challenging to realize on other platforms. While the full advantage of digital quantum simulation can only be realized with quantum error correction and fault-tolerant quantum computing, recent progress, including the present study, demonstrate already encouraging capabilities on rapidly advancing NISQ-era hardware. As a final remark, we point out that, while we have focused on the quantum simulation of a 2D Chern insulator, our mapping method is general to arbitrary d -dimensional, n -band one-body systems (see Sec. S1 of Supplemental Material [98]) and is readily applicable to study more sophisticated topological phenomena [77,78,144–151].

J. M. K. and T. T. thank Wei En Ng and Yong Han Phee of the National University of Singapore for discussions

on the quantum simulation implementation. This work is supported by the Singapore National Research Foundation Grant No. NRF2021-QEP2-02-P09. The authors acknowledge the use of IBM Quantum services for this work. The views expressed are those of the authors and do not reflect the official policy or position of IBM or the IBM Quantum team.

*phylch@nus.edu.sg

- [1] B. I. Halperin, Quantized Hall conductance, current-carrying edge states, and the existence of extended states in a two-dimensional disordered potential, *Phys. Rev. B* **25**, 2185 (1982).
- [2] A. H. MacDonald and P. Středa, Quantized Hall effect and edge currents, *Phys. Rev. B* **29**, 1616 (1984).
- [3] F. D. M. Haldane, Model for a Quantum Hall Effect without Landau Levels: Condensed-Matter Realization of the “Parity Anomaly,” *Phys. Rev. Lett.* **61**, 2015 (1988).
- [4] C.-X. Liu, X.-L. Qi, X. Dai, Z. Fang, and S.-C. Zhang, Quantum Anomalous Hall Effect in $hg_{1-y}mn_yTe$ Quantum Wells, *Phys. Rev. Lett.* **101**, 146802 (2008).
- [5] R. Yu, W. Zhang, H.-J. Zhang, S.-C. Zhang, X. Dai, and Z. Fang, Quantized anomalous Hall effect in magnetic topological insulators, *Science* **329**, 61 (2010).
- [6] C.-Z. Chang, J. Zhang, X. Feng, J. Shen, Z. Zhang, M. Guo, K. Li, Y. Ou, P. Wei, L.-L. Wang *et al.*, Experimental observation of the quantum anomalous Hall effect in a magnetic topological insulator, *Science* **340**, 167 (2013).
- [7] Y.-F. Zhao, R. Zhang, R. Mei, L.-J. Zhou, H. Yi, Y.-Q. Zhang, J. Yu, R. Xiao, K. Wang, N. Samarth *et al.*, Tuning the Chern number in quantum anomalous Hall insulators, *Nature (London)* **588**, 419 (2020).
- [8] F. R. Geisenhof, F. Winterer, A. M. Seiler, J. Lenz, T. Xu, F. Zhang, and R. T. Weitz, Quantum anomalous Hall octet driven by orbital magnetism in bilayer graphene, *Nature (London)* **598**, 53 (2021).
- [9] C. Tschirhart, M. Serlin, H. Polshyn, A. Shragai, Z. Xia, J. Zhu, Y. Zhang, K. Watanabe, T. Taniguchi, M. Huber *et al.*, Imaging orbital ferromagnetism in a moiré Chern insulator, *Science* **372**, 1323 (2021).
- [10] M. Serlin, C. Tschirhart, H. Polshyn, Y. Zhang, J. Zhu, K. Watanabe, T. Taniguchi, L. Balents, and A. Young, Intrinsic quantized anomalous Hall effect in a moiré heterostructure, *Science* **367**, 900 (2020).
- [11] A. L. Sharpe, E. J. Fox, A. W. Barnard, J. Finney, K. Watanabe, T. Taniguchi, M. Kastner, and D. Goldhaber-Gordon, Emergent ferromagnetism near three-quarters filling in twisted bilayer graphene, *Science* **365**, 605 (2019).
- [12] G. Chen, A. L. Sharpe, E. J. Fox, Y.-H. Zhang, S. Wang, L. Jiang, B. Lyu, H. Li, K. Watanabe, T. Taniguchi *et al.*, Tunable correlated Chern insulator and ferromagnetism in a moiré superlattice, *Nature (London)* **579**, 56 (2020).
- [13] H. Polshyn, J. Zhu, M. A. Kumar, Y. Zhang, F. Yang, C. L. Tschirhart, M. Serlin, K. Watanabe, T. Taniguchi, A. H. MacDonald *et al.*, Electrical switching of magnetic order in an orbital Chern insulator, *Nature (London)* **588**, 66 (2020).

- [14] Y.-H. Zhang, D. Mao, Y. Cao, P. Jarillo-Herrero, and T. Senthil, Nearly flat Chern bands in moiré superlattices, *Phys. Rev. B* **99**, 075127 (2019).
- [15] F. D. M. Haldane and S. Raghu, Possible Realization of Directional Optical Waveguides in Photonic Crystals with Broken Time-Reversal Symmetry, *Phys. Rev. Lett.* **100**, 013904 (2008).
- [16] J.-X. Fu, R.-J. Liu, and Z.-Y. Li, Robust one-way modes in gyromagnetic photonic crystal waveguides with different interfaces, *Appl. Phys. Lett.* **97**, 041112 (2010).
- [17] Z. Wang, Y. Chong, J. Joannopoulos, and M. Soljačić, Observation of unidirectional backscattering-immune topological electromagnetic states, *Nature (London)* **461**, 772 (2009).
- [18] J. Y. Lin, N. C. Hu, Y. J. Chen, C. H. Lee, and X. Zhang, Line nodes, Dirac points, and Lifshitz transition in two-dimensional nonsymmorphic photonic crystals, *Phys. Rev. B* **96**, 075438 (2017).
- [19] V. Peano, C. Brendel, M. Schmidt, and F. Marquardt, Topological Phases of Sound and Light, *Phys. Rev. X* **5**, 031011 (2015).
- [20] L. Lu, J. D. Joannopoulos, and M. Soljačić, Topological photonics, *Nat. Photonics* **8**, 821 (2014).
- [21] A. B. Khanikaev and G. Shvets, Two-dimensional topological photonics, *Nat. Photonics* **11**, 763 (2017).
- [22] T. Ozawa, H. M. Price, A. Amo, N. Goldman, M. Hafezi, L. Lu, M. C. Rechtsman, D. Schuster, J. Simon, O. Zilberberg *et al.*, Topological photonics, *Rev. Mod. Phys.* **91**, 015006 (2019).
- [23] D. Smirnova, D. Leykam, Y. Chong, and Y. Kivshar, Nonlinear topological photonics, *Appl. Phys. Rev.* **7**, 021306 (2020).
- [24] S. Klembt, T. Harder, O. Egorov, K. Winkler, R. Ge, M. Bandres, M. Emmerling, L. Worschech, T. Liew, M. Segev *et al.*, Exciton-polariton topological insulator, *Nature (London)* **562**, 552 (2018).
- [25] Y. V. Kartashov and D. V. Skryabin, Two-Dimensional Topological Polariton Laser, *Phys. Rev. Lett.* **122**, 083902 (2019).
- [26] S. Mandal, R. Banerjee, E. A. Ostrovskaya, and T. C. H. Liew, Nonreciprocal Transport of Exciton Polaritons in a Non-Hermitian Chain, *Phys. Rev. Lett.* **125**, 123902 (2020).
- [27] R. Su, S. Ghosh, T. C. Liew, and Q. Xiong, Optical switching of topological phase in a perovskite polariton lattice, *Sci. Adv.* **7**, eabf8049 (2021).
- [28] C. Kane and T. Lubensky, Topological boundary modes in isostatic lattices, *Nat. Phys.* **10**, 39 (2014).
- [29] L. M. Nash, D. Kleckner, A. Read, V. Vitelli, A. M. Turner, and W. T. Irvine, Topological mechanics of gyroscopic metamaterials, *Proc. Natl. Acad. Sci. U.S.A.* **112**, 14495 (2015).
- [30] C. H. Lee, G. Li, G. Jin, Y. Liu, and X. Zhang, Topological dynamics of gyroscopic and Floquet lattices from Newton's laws, *Phys. Rev. B* **97**, 085110 (2018).
- [31] A. B. Khanikaev, R. Fleury, S. H. Mousavi, and A. Alu, Topologically robust sound propagation in an angular-momentum-biased graphene-like resonator lattice, *Nat. Commun.* **6**, 8260 (2015).
- [32] P. Wang, L. Lu, and K. Bertoldi, Topological Phononic Crystals with One-Way Elastic Edge Waves, *Phys. Rev. Lett.* **115**, 104302 (2015).
- [33] R. Süssstrunk and S. D. Huber, Observation of phononic helical edge states in a mechanical topological insulator, *Science* **349**, 47 (2015).
- [34] C. He, X. Ni, H. Ge, X.-C. Sun, Y.-B. Chen, M.-H. Lu, X.-P. Liu, and Y.-F. Chen, Acoustic topological insulator and robust one-way sound transport, *Nat. Phys.* **12**, 1124 (2016).
- [35] Y. Guo, R. M. Kroese, B. P. Marsh, S. Gopalakrishnan, J. Keeling, and B. L. Lev, An optical lattice with sound, *Nature (London)* **599**, 211 (2021).
- [36] T. Hofmann, T. Helbig, C. H. Lee, M. Greiter, and R. Thomale, Chiral Voltage Propagation and Calibration in a Topoelectrical Chern Circuit, *Phys. Rev. Lett.* **122**, 247702 (2019).
- [37] C. H. Lee, S. Imhof, C. Berger, F. Bayer, J. Brehm, L. W. Molenkamp, T. Kiessling, and R. Thomale, Topoelectrical circuits, *Commun. Phys.* **1**, 1 (2018).
- [38] J. Ningyuan, C. Owens, A. Sommer, D. Schuster, and J. Simon, Time- and Site-Resolved Dynamics in a Topological Circuit, *Phys. Rev. X* **5**, 021031 (2015).
- [39] T. Helbig, T. Hofmann, C. H. Lee, R. Thomale, S. Imhof, L. W. Molenkamp, and T. Kiessling, Band structure engineering and reconstruction in electric circuit networks, *Phys. Rev. B* **99**, 161114(R) (2019).
- [40] V. V. Albert, L. I. Glazman, and L. Jiang, Topological Properties of Linear Circuit Lattices, *Phys. Rev. Lett.* **114**, 173902 (2015).
- [41] W. Cai, J. Han, F. Mei, Y. Xu, Y. Ma, X. Li, H. Wang, Y. P. Song, Z.-Y. Xue, Z.-Q. Yin, S. Jia, and L. Sun, Observation of Topological Magnon Insulator States in a Superconducting Circuit, *Phys. Rev. Lett.* **123**, 080501 (2019).
- [42] M. Ezawa, Non-Hermitian higher-order topological states in nonreciprocal and reciprocal systems with their electric-circuit realization, *Phys. Rev. B* **99**, 201411(R) (2019).
- [43] Z.-Q. Zhang, B.-L. Wu, J. Song, and H. Jiang, Topological Anderson insulator in electric circuits, *Phys. Rev. B* **100**, 184202 (2019).
- [44] N. A. Olekhno, E. I. Kretov, A. A. Stepanenko, P. A. Ivanova, V. V. Yaroshenko, E. M. Puhtina, D. S. Filonov, B. Cappello, L. Matekovits, and M. A. Gorlach, Topological edge states of interacting photon pairs emulated in a topoelectrical circuit, *Nat. Commun.* **11**, 1436 (2020).
- [45] C. H. Lee, A. Sutrisno, T. Hofmann, T. Helbig, Y. Liu, Y. S. Ang, L. K. Ang, X. Zhang, M. Greiter, and R. Thomale, Imaging nodal knots in momentum space through topoelectrical circuits, *Nat. Commun.* **11**, 1 (2020).
- [46] M. Ezawa, Topological Euler insulators and their electric circuit realization, *Phys. Rev. B* **103**, 205303 (2021).
- [47] A. Stegmaier, S. Imhof, T. Helbig, T. Hofmann, C. H. Lee, M. Kremer, A. Fritzsche, T. Feichtner, S. Klembt, S. Höfling *et al.*, Topological Defect Engineering and PT Symmetry in Non-Hermitian Electrical Circuits, *Phys. Rev. Lett.* **126**, 215302 (2021).
- [48] D. Zou, T. Chen, W. He, J. Bao, C. H. Lee, H. Sun, and X. Zhang, Observation of hybrid higher-order skin-topological effect in non-Hermitian topoelectrical circuits, *Nat. Commun.* **12**, 7201 (2021).

- [49] C. Shang, S. Liu, R. Shao, P. Han, X. Zang, X. Zhang, K. N. Salama, W. Gao, C. H. Lee, R. Thomale *et al.*, Experimental identification of the second-order non-Hermitian skin effect with physics-graph-informed machine learning, [arXiv:2203.00484](#).
- [50] X. Zhang, B. Zhang, H. Sahin, Z. B. Siu, S. Rafi-Ul-Islam, J. F. Kong, M. Jalil, R. Thomale, and C. H. Lee, Anomalous fractal scaling in two-dimensional electric networks, [arXiv:2204.05329](#).
- [51] H. Yang, L. Song, Y. Cao, and P. Yan, Experimental realization of two-dimensional weak topological insulators, *Nano Lett.* **22**, 3125 (2022).
- [52] H. Hohmann, T. Hofmann, T. Helbig, S. Imhof, H. Brand, L. K. Upreti, A. Stegmaier, A. Fritzsche, T. Müller, U. Schwingenschlögl *et al.*, Observation of cnoidal wave localization in non-linear topoelectric circuits, [arXiv:2206.09931](#).
- [53] Y. Liu, H. Yang, X. Wang, Z.-X. Li, and Y. Cao, Observation of symmetry-protected corner states in breathing honeycomb topoelectrical circuits, *J. Appl. Phys.* **131**, 094903 (2022).
- [54] E. Altman *et al.*, Quantum simulators: Architectures and opportunities, *PRX Quantum* **2**, 017003 (2021).
- [55] K. Choo, C. W. von Keyserlingk, N. Regnault, and T. Neupert, Measurement of the Entanglement Spectrum of a Symmetry-Protected Topological State Using the IBM Quantum Computer, *Phys. Rev. Lett.* **121**, 086808 (2018).
- [56] A. Smith, B. Jobst, A. G. Green, and F. Pollmann, Crossing a topological phase transition with a quantum computer, *Phys. Rev. Research* **4**, L022020 (2022).
- [57] D. Azses, R. Haenel, Y. Naveh, R. Raussendorf, E. Sela, and E. G. Dalla Torre, Identification of Symmetry-Protected Topological States on Noisy Quantum Computers, *Phys. Rev. Lett.* **125**, 120502 (2020).
- [58] F. Mei, Q. Guo, Y.-F. Yu, L. Xiao, S.-L. Zhu, and S. Jia, Digital Simulation of Topological Matter on Programmable Quantum Processors, *Phys. Rev. Lett.* **125**, 160503 (2020).
- [59] J. M. Koh, T. Tai, Y. H. Phee, W. E. Ng, and C. H. Lee, Stabilizing multiple topological fermions on a quantum computer, *npj Quantum Inf.* **8**, 16 (2022).
- [60] A. T. Tan, S.-N. Sun, R. N. Tazhilov, G. K. Chan, and A. J. Minnich, Realizing symmetry-protected topological phases in a spin-1/2 chain with next-nearest neighbor hopping on superconducting qubits, [arXiv:2112.10333](#).
- [61] H.-S. Zhong *et al.*, Quantum computational advantage using photons, *Science* **370**, 1460 (2020).
- [62] K. J. Satzinger *et al.*, Realizing topologically ordered states on a quantum processor, *Science* **374**, 1237 (2021).
- [63] G. A. Quantum *et al.*, Hartree-fock on a superconducting qubit quantum computer, *Science* **369**, 1084 (2020).
- [64] A. Chiesa, F. Tacchino, M. Grossi, P. Santini, I. Tavernelli, D. Gerace, and S. Carretta, Quantum hardware simulating four-dimensional inelastic neutron scattering, *Nat. Phys.* **15**, 455 (2019).
- [65] F. Arute *et al.*, Quantum supremacy using a programmable superconducting processor, *Nature (London)* **574**, 505 (2019).
- [66] S. A. Moses, J. P. Covey, M. T. Miecnikowski, D. S. Jin, and J. Ye, New frontiers for quantum gases of polar molecules, *Nat. Phys.* **13**, 13 (2017).
- [67] L. R. Liu, J. D. Hood, Y. Yu, J. T. Zhang, K. Wang, Y.-W. Lin, T. Rosenband, and K.-K. Ni, Molecular Assembly of Ground-State Cooled Single Atoms, *Phys. Rev. X* **9**, 021039 (2019).
- [68] R. Samajdar, W. W. Ho, H. Pichler, M. D. Lukin, and S. Sachdev, Quantum phases of Rydberg atoms on a kagome lattice, *Proc. Natl. Acad. Sci. U.S.A.* **118**, e2015785118 (2021).
- [69] S. de Léséleuc, V. Lienhard, P. Scholl, D. Barredo, S. Weber, N. Lang, H. P. Büchler, T. Lahaye, and A. Browaeys, Observation of a symmetry-protected topological phase of interacting bosons with Rydberg atoms, *Science* **365**, 775 (2019).
- [70] S. Ebadi, T. T. Wang, H. Levine, A. Keesling, G. Semeghini, A. Omran, D. Bluvstein, R. Samajdar, H. Pichler, W. W. Ho *et al.*, Quantum phases of matter on a 256-atom programmable quantum simulator, *Nature (London)* **595**, 227 (2021).
- [71] J. Preskill, Quantum computing in the NISQ era and beyond, *Quantum* **2**, 79 (2018).
- [72] A. Kandala, K. Temme, A. D. Córcoles, A. Mezzacapo, J. M. Chow, and J. M. Gambetta, Error mitigation extends the computational reach of a noisy quantum processor, *Nature (London)* **567**, 491 (2019).
- [73] A. Kandala, A. Mezzacapo, K. Temme, M. Takita, M. Brink, J. M. Chow, and J. M. Gambetta, Hardware-efficient variational quantum eigensolver for small molecules and quantum magnets, *Nature (London)* **549**, 242 (2017).
- [74] K. Temme, S. Bravyi, and J. M. Gambetta, Error Mitigation for Short-Depth Quantum Circuits, *Phys. Rev. Lett.* **119**, 180509 (2017).
- [75] M. Cerezo, A. Arrasmith, R. Babbush, S. C. Benjamin, S. Endo, K. Fujii, J. R. McClean, K. Mitarai, X. Yuan, L. Cincio *et al.*, Variational quantum algorithms, *Nat. Rev. Phys.* **3**, 625 (2021).
- [76] B. Heim, M. Soeken, S. Marshall, C. Granade, M. Roetteler, A. Geller, M. Troyer, and K. Svore, Quantum programming languages, *Nat. Rev. Phys.* **2**, 709 (2020).
- [77] A. Kirmani, K. Bull, C.-Y. Hou, V. Saravanan, S. M. Saeed, Z. Papić, A. Rahmani, and P. Ghaemi, Probing Geometric Excitations of Fractional Quantum Hall States on Quantum Computers, *Phys. Rev. Lett.* **129**, 056801 (2022).
- [78] A. Rahmani, K. J. Sung, H. Puterman, P. Roushan, P. Ghaemi, and Z. Jiang, Creating and manipulating a Laughlin-type $\nu = 1/3$ fractional quantum Hall state on a quantum computer with linear depth circuits, *PRX Quantum* **1**, 020309 (2020).
- [79] A. Smith, M. S. Kim, F. Pollmann, and J. Knolle, Simulating quantum many-body dynamics on a current digital quantum computer, *npj Quantum Inf.* **5**, 106 (2019).
- [80] D. Zhu, S. Johri, N. H. Nguyen, C. H. Alderete, K. A. Landsman, N. M. Linke, C. Monroe, and A. Y. Matsuura, Probing many-body localization on a noisy quantum computer, *Phys. Rev. A* **103**, 032606 (2021).

- [81] A. Cervera-Lierta, Exact Ising model simulation on a quantum computer, *Quantum* **2**, 114 (2018).
- [82] D. Paulson, L. Dellantonio, J. F. Haase, A. Celi, A. Kan, A. Jena, C. Kokail, R. van Bijnen, K. Jansen, P. Zoller *et al.*, Simulating 2D effects in lattice gauge theories on a quantum computer, *PRX Quantum* **2**, 030334 (2021).
- [83] X. Mi, M. Ippoliti, C. Quintana, A. Greene, Z. Chen, J. Gross, F. Arute, K. Arya, J. Atalaya, R. Babbush *et al.*, Time-crystalline eigenstate order on a quantum processor, *Nature (London)* **601**, 531 (2022).
- [84] This Letter serves to 2D 1-body Chern phenomena by mapping to a 1D 2-body problem, while a few existing theoretical and experimental works aims to understanding other 1D 2-body systems by studying 2 1-body setups [44,85–87].
- [85] S. Longhi and G. Della Valle, Tamm-Hubbard surface states in the continuum, *J. Phys. Condens. Matter* **25**, 235601 (2013).
- [86] S. Mukherjee, M. Valiente, N. Goldman, A. Spracklen, E. Andersson, P. Öhberg, and R. R. Thomson, Observation of pair tunneling and coherent destruction of tunneling in arrays of optical waveguides, *Phys. Rev. A* **94**, 053853 (2016).
- [87] M. Gorlach, M. Di Liberto, A. Recati, I. Carusotto, A. Poddubny, and C. Menotti, Analogue simulation of two-body quantum dynamics with classical setup, *J. Phys. Conf. Ser.* **1092**, 012045 (2018).
- [88] V. Havlíček, A. D. Cárcoles, K. Temme, A. W. Harrow, A. Kandala, J. M. Chow, and J. M. Gambetta, Supervised learning with quantum-enhanced feature spaces, *Nature (London)* **567**, 209 (2019).
- [89] J. M. Koh, S.-N. Sun, M. Motta, and A. J. Minnich, Experimental realization of a measurement-induced entanglement phase transition on a superconducting quantum processor, [arXiv:2203.04338](https://arxiv.org/abs/2203.04338).
- [90] A. J. McCaskey, Z. P. Parks, J. Jakowski, S. V. Moore, T. D. Morris, T. S. Humble, and R. C. Pooser, Quantum chemistry as a benchmark for near-term quantum computers, *npj Quantum Inf.* **5**, 99 (2019).
- [91] S. E. Smart and D. A. Mazziotti, Efficient two-electron ansatz for benchmarking quantum chemistry on a quantum computer, *Phys. Rev. Research* **2**, 023048 (2020).
- [92] A. A. Zhukov, S. V. Remizov, W. V. Pogosov, and Y. E. Lozovik, Algorithmic simulation of far-from-equilibrium dynamics using quantum computer, *Quantum Inf. Process.* **17**, 223 (2018).
- [93] D. J. Thouless, M. Kohmoto, M. P. Nightingale, and M. den Nijs, Quantized Hall Conductance in a Two-Dimensional Periodic Potential, *Phys. Rev. Lett.* **49**, 405 (1982).
- [94] Assuming a minimum of 5–7 unit cells in each 2D direction, with two sites per unit cell.
- [95] K. Sun, Z. Gu, H. Katsura, and S. Das Sarma, Nearly Flatbands with Nontrivial Topology, *Phys. Rev. Lett.* **106**, 236803 (2011).
- [96] C. H. Lee and X.-L. Qi, Lattice construction of pseudo-potential Hamiltonians for fractional Chern insulators, *Phys. Rev. B* **90**, 085103 (2014).
- [97] N. Regnault and B. A. Bernevig, Fractional Chern Insulator, *Phys. Rev. X* **1**, 021014 (2011).
- [98] See Supplemental Material at <http://link.aps.org/supplemental/10.1103/PhysRevLett.129.140502> for Secs. S1 to S3, supplemental figures and technical details, which includes Refs. [99–120]
- [99] D. R. Hofstadter, Energy levels and wave functions of Bloch electrons in rational and irrational magnetic fields, *Phys. Rev. B* **14**, 2239 (1976).
- [100] K. v. Klitzing, G. Dorda, and M. Pepper, New Method for High-Accuracy Determination of the Fine-Structure Constant Based on Quantized Hall Resistance, *Phys. Rev. Lett.* **45**, 494 (1980).
- [101] R. B. Laughlin, Quantized Hall conductivity in two dimensions, *Phys. Rev. B* **23**, 5632 (1981).
- [102] D. J. Thouless, Quantization of particle transport, *Phys. Rev. B* **27**, 6083 (1983).
- [103] N. Regnault and B. A. Bernevig, Fractional Chern Insulator, *Phys. Rev. X* **1**, 021014 (2011).
- [104] C. Fan and F. Y. Wu, General lattice model of phase transitions, *Phys. Rev. B* **2**, 723 (1970).
- [105] J. Ginibre, Existence of phase transitions for quantum lattice systems, *Commun. Math. Phys.* **14**, 205 (1969).
- [106] H. F. Trotter, On the product of semi-groups of operators, *Proc. Am. Math. Soc.* **10**, 545 (1959).
- [107] I. Montvay and G. Münster, *Quantum Fields on a Lattice* (Cambridge University Press, Cambridge, England, 1997).
- [108] R. Malouf, A comparison of algorithms for maximum entropy parameter estimation, in *Proceedings of the 6th Conference on Natural Language Learning, COLING-02* (Association for Computational Linguistics, U.S., 2002), Vol. 20, pp. 1–7.
- [109] G. Vidal, Efficient Simulation of One-Dimensional Quantum Many-Body Systems, *Phys. Rev. Lett.* **93**, 040502 (2004).
- [110] N. Hatano and M. Suzuki, Finding exponential product formulas of higher orders, in *Quantum Annealing and Other Optimization Methods*, edited by A. Das and B. K. Chakrabarti (Springer, Berlin, Heidelberg, 2005), pp. 37–68.
- [111] G. Andrew and J. Gao, Scalable training of L1-regularized log-linear models, in *International Conference on Machine Learning* (2007).
- [112] N. Moll, P. Barkoutsos, L. S. Bishop, J. M. Chow, A. Cross, D. J. Egger, S. Filipp, A. Fuhrer, J. M. Gambetta, M. Ganzhorn *et al.*, Quantum optimization using variational algorithms on near-term quantum devices, *Quantum Sci. Technol.* **3**, 030503 (2018).
- [113] U. Alvarez-Rodríguez, M. Sanz, L. Lamata, and E. Solano, Quantum artificial life in an IBM quantum computer, *Sci. Rep.* **8**, 14793 (2018).
- [114] B. K. Behera, T. Reza, A. Gupta, and P. K. Panigrahi, Designing quantum router in IBM quantum computer, *Quantum Inf. Process.* **18**, 328 (2019).
- [115] L. M. Sieberer, T. Olsacher, A. Elben, M. Heyl, P. Hauke, F. Haake, and P. Zoller, Digital quantum simulation, Trotter errors, and quantum chaos of the kicked top, *npj Quantum Inf.* **5**, 78 (2019).
- [116] M. Heyl, P. Hauke, and P. Zoller, Quantum localization bounds Trotter errors in digital quantum simulation, *Sci. Adv.* **5**, eaau8342 (2019).
- [117] A. W. Cross, L. S. Bishop, S. Sheldon, P. D. Nation, and J. M. Gambetta, Validating quantum computers using

- randomized model circuits, *Phys. Rev. A* **100**, 032328 (2019).
- [118] M. Motta, C. Sun, A. T. Tan, M. J. O'Rourke, E. Ye, A. J. Minnich, F. G. Brandão, and G. K.-L. Chan, Determining eigenstates and thermal states on a quantum computer using quantum imaginary time evolution, *Nat. Phys.* **16**, 205 (2020).
- [119] T. Jones and S. C. Benjamin, Robust quantum compilation and circuit optimisation via energy minimisation, *Quantum* **6**, 628 (2022).
- [120] S. Andersson *et al.*, Learn quantum computation using QISKit (2020), <https://qisKit.org/textbook/>.
- [121] G. Wirth, M. Ölschläger, and A. Hemmerich, Evidence for orbital superfluidity in the P-band of a bipartite optical square lattice, *Nat. Phys.* **7**, 147 (2011).
- [122] R. Landig, L. Hrúby, N. Dogra, M. Landini, R. Mottl, T. Donner, and T. Esslinger, Quantum phases from competing short-and long-range interactions in an optical lattice, *Nature (London)* **532**, 476 (2016).
- [123] T. Paananen and T. Dahm, Topological flat bands in optical checkerboardlike lattices, *Phys. Rev. A* **91**, 033604 (2015).
- [124] M. Ölschläger, G. Wirth, and A. Hemmerich, Unconventional Superfluid Order in the f Band of a Bipartite Optical Square Lattice, *Phys. Rev. Lett.* **106**, 015302 (2011).
- [125] K. Baumann, R. Mottl, F. Brennecke, and T. Esslinger, Exploring Symmetry Breaking at the Dicke Quantum Phase Transition, *Phys. Rev. Lett.* **107**, 140402 (2011).
- [126] \mathcal{F} is a measure of the topological charge, giving a Chern number of $C = \int_{-\pi}^{\pi} \int_{-\pi}^{\pi} \mathcal{F} dk_1 dk_2 / 2\pi = 2$, as expected.
- [127] R. Yu, X. L. Qi, A. Bernevig, Z. Fang, and X. Dai, Equivalent expression of F_2 topological invariant for band insulators using the non-Abelian berry connection, *Phys. Rev. B* **84**, 075119 (2011).
- [128] R. Resta, Quantum-Mechanical Position Operator in Extended Systems, *Phys. Rev. Lett.* **80**, 1800 (1998).
- [129] C. H. Lee and P. Ye, Free-fermion entanglement spectrum through Wannier interpolation, *Phys. Rev. B* **91**, 085119 (2015).
- [130] A. Nelson, T. Neupert, T. Bzdušek, and A. Alexandradinata, Multicellularity of Delicate Topological Insulators, *Phys. Rev. Lett.* **126**, 216404 (2021).
- [131] G. García-Pérez, M. A. Rossi, and S. Maniscalco, IBM Q experience as a versatile experimental testbed for simulating open quantum systems, *npj Quantum Inf.* **6**, 1 (2020).
- [132] A. Cross, The IBM Q experience and QISKit open-source quantum computing software, in *APS March Meeting Abstracts* (2018), Vol. 2018, pp. L58–003, <http://meetings.aps.org/link/BAPS.2018.MAR.L58.3>.
- [133] G. Aleksandrowicz *et al.*, QISKit: An open-source framework for quantum computing, Zenodo, [10.5281/ZENODO.2562111](https://doi.org/10.5281/ZENODO.2562111)(2019).
- [134] I. M. Georgescu, S. Ashhab, and F. Nori, Quantum simulation, *Rev. Mod. Phys.* **86**, 153 (2014).
- [135] G. Ortiz, J. E. Gubernatis, E. Knill, and R. Laflamme, Quantum algorithms for fermionic simulations, *Phys. Rev. A* **64**, 022319 (2001).
- [136] S. Imhof, C. Berger, F. Bayer, J. Brehm, L. W. Molenkamp, T. Kiessling, F. Schindler, C. H. Lee, M. Greiter, T. Neupert *et al.*, Topoelectrical-circuit realization of topological corner modes, *Nat. Phys.* **14**, 925 (2018).
- [137] Y. Wang, L.-J. Lang, C. H. Lee, B. Zhang, and Y. Chong, Topologically enhanced harmonic generation in a non-linear transmission line metamaterial, *Nat. Commun.* **10**, 1 (2019).
- [138] S.-N. Sun, M. Motta, R. N. Tazhigulov, A. T. K. Tan, Garnet Kin-Lic Chan, and A. J. Minnich, Quantum computation of finite-temperature static and dynamical properties of spin systems using quantum imaginary time evolution, *PRX Quantum* **2**, 010317 (2021).
- [139] S. Khatri, R. LaRose, A. Poremba, L. Cincio, A. T. Sornborger, and P. J. Coles, Quantum-assisted quantum compiling, *Quantum* **3**, 140 (2019).
- [140] K. Heya, Y. Suzuki, Y. Nakamura, and K. Fujii, Variational quantum gate optimization, [arXiv:1810.12745](https://arxiv.org/abs/1810.12745).
- [141] J. Gray, QUIMB: A PYTHON package for quantum information and many-body calculations, *J. Open Source Software* **3**, 819 (2018).
- [142] S. McArdle, X. Yuan, and S. Benjamin, Error-Mitigated Digital Quantum Simulation, *Phys. Rev. Lett.* **122**, 180501 (2019).
- [143] C. H. Lee, Many-body topological and skin states without open boundaries, *Phys. Rev. B* **104**, 195102 (2021).
- [144] C. H. Lee, Z. Papić, and R. Thomale, Geometric Construction of Quantum Hall Clustering Hamiltonians, *Phys. Rev. X* **5**, 041003 (2015).
- [145] X.-D. Chen, W.-M. Deng, F.-L. Shi, F.-L. Zhao, M. Chen, and J.-W. Dong, Direct Observation of Corner States in Second-Order Topological Photonic Crystal Slabs, *Phys. Rev. Lett.* **122**, 233902 (2019).
- [146] Y. Gu, C. H. Lee, X. Wen, G. Y. Cho, S. Ryu, and X.-L. Qi, Holographic duality between $(2+1)$ -dimensional quantum anomalous Hall state and $(3+1)$ -dimensional topological insulators, *Phys. Rev. B* **94**, 125107 (2016).
- [147] T. Tuloup, R. W. Bomantara, C. H. Lee, and J. Gong, Nonlinearity induced topological physics in momentum space and real space, *Phys. Rev. B* **102**, 115411 (2020).
- [148] C. W. Peterson, T. Li, W. A. Benalcazar, T. L. Hughes, and G. Bahl, A fractional corner anomaly reveals higher-order topology, *Science* **368**, 1114 (2020).
- [149] C. H. Lee, Y. Wang, Y. Chen, and X. Zhang, Electromagnetic response of quantum Hall systems in dimensions five and six and beyond, *Phys. Rev. B* **98**, 094434 (2018).
- [150] Z. Yang, E. Lustig, Y. Lumer, and M. Segev, Photonic Floquet topological insulators in a fractal lattice, *Light* **9**, 1 (2020).
- [151] For example, the paradigmatic Hofstadter model, which contains hopping with more general site-dependent phase factors on a rectangular lattice in comparison to the presently considered checkerboard model. We provide a discussion of its mapping and implementation in Ref. [98].